Active Shape Analysis of Mandibular Growth

Klaus B. Hilger[1], Rasmus Larsen[1], Sven Kreiborg[2],
Søren Krarup[2], Tron A. Darvann[1,2], and Jeffrey L. Marsh[3]

[1]Informatics and Mathematical Modelling, Technical University of Denmark,
IMM, DTU, Richard Petersens Plads, Building 321, DK-2800 Kgs. Lyngby, Denmark
[2]3D-Laboratory, Department of Pediatric Dentistry and Clinical Genetics, School of
Dentistry, University of Copenhagen, DK-2200 Copenhagen N, Denmark
[3]Department of Pediatric Plastic Surgery, St. Louis Children's Hospital, Washington
University School of Medicine, St. Louis, Missouri, USA
kbh@imm.dtu.dk, http://www.imm.dtu.dk/~kbh/

Abstract. This work contains a clinical validation using biological landmarks of a Geometry Constrained Diffusion registration of mandibular surfaces. Canonical Correlations Analysis is extended to analyse 3D landmarks and the correlations are used as similarity measures for landmark clustering. A novel Active Shape Model is proposed targeting growth modelling by applying Partial Least Squares regression in decomposing the Procrustes tangent space. Shape centroid size is applied as dependent variable but the method generalizes to handle other, both uni- and multivariate, effects probing for high covariation wrt. shape variation.

1 Introduction

This work is primarily based on the theory of point distribution models, which are widely used in modelling biological shape variability over a set of annotated training data, [6, 7], based on generalized Procrustes alignment, [10], and decomposition, [16], in shape tangent space. The data are mandibular surfaces acquired from computed tomography (CT) scans of subjects with Apert syndrome. All scans are acquired for treatment and diagnostics purposes. In Apert syndrome, the mandible is not affected by the primary anomaly, [15]. In [1] the data are applied in a Geometry Constrained Diffusion (GCD) registration and a subsequent Principal Component (PCA) based growth analysis. A subset of the mandibles are annotated using 32 biological landmarks placed on distinct skeletal features in the CT volume. The landmarks are applied in this study to evaluate the dense correspondence obtained by GCD. Moreover, additional subjects with Apert syndrome are included into the data set, now representing 10 subjects, five males and five females, scanned at ages from 1 month to 14 years of age. Since the subjects are prepubescent and the sample size is small, the sexes are pooled in the subsequent analyses. The resulting data set consists of 36 CT scans. The remaining paper is organized in three sections. Section 2 contains an evaluation of the GCD based correspondence and an analysis of the underlying distribution of the biological landmarks. Section 3 presents derived Active Shape Models (ASM) of the biological landmarks that correlate to growth. In Section 4 we summarize and give some concluding remarks.

2 Clinical Validation of GCD Obtained Correspondence

Geometry Constrained Diffusion is a method for non-rigid registration, see [1, 2], and the related work on Brownian Warps, [17]. GCD of a deformation field $\boldsymbol{D}: \mathbb{R}^3 \rightarrow \mathbb{R}^3$ mapping the surface $\boldsymbol{S}_s$ onto the surface $\boldsymbol{S}_t$ is given by

$$\partial_t \boldsymbol{D} = \begin{cases} \Delta \boldsymbol{D} - \boldsymbol{n}_{S_t} \frac{\boldsymbol{n}_{S_t}^T \Delta \boldsymbol{D}}{||\boldsymbol{n}_{S_t}||^2} & \text{if } \boldsymbol{x} \in \boldsymbol{S}_s \\ \Delta \boldsymbol{D} & \text{if } \boldsymbol{x} \notin \boldsymbol{S}_s \end{cases} \tag{1}$$

where $\boldsymbol{n}_{S_t}$ is the unit surface normal of $\boldsymbol{S}_t(\boldsymbol{D}(\boldsymbol{x}) + \boldsymbol{x})$. Thus, GCD is a numerical scheme for solving a space and time discretized version of the heat equation on the deformation field with certain boundary conditions. It solves the aperture and 3D interpolation problem simultaneously by finding the simplest displacement field. To validate the correspondences obtained by GCD, the first task is to bring the biological landmarks of the CT scanning onto the manually segmented, smoothed, skeletal surfaces applied in [1]. For this we apply the Iterative Closest Point (ICP) algorithm introduced in [3]. Given L landmarks $\{\boldsymbol{x}_i\}_{i=1}^L$ on a source shape the ICP algorithm finds the similarity transformations that minimize the sum of squared point to surface residuals between the source and the target shape. By applying the ICP algorithm we recover the rigid transformation that brings the biological landmarks closest to the corresponding segmented mandibular surfaces. Finally, to find the correspondence of the landmarks on the surfaces we allow a free deformation of the data by applying closest point on surface projection. The annotation of the biological landmarks and the segmentation and smoothing of the mandibular surfaces are performed by independent observers. For young mandibles the gradient between bone and soft-tissue is not as well defined as for older mandibles. This constitute a source of variation in the inter-observer segmentation and labeling performance. In evaluating the GCD registration the landmarks located on the oldest mandible are used as master references for the earlier scans. This is done to account for subject specific variation. To map the patient specific master landmarks onto younger mandibles we use barycentric coordinates within the fine scale GCD polygonized representation of the shapes. In Table 1 the residual distances are shown between the barycentric master landmarks and the reconstructed landmarks at various ages for the six patients studied in [1]. The errors thus measure the agreement between the biological landmarks and the correspondence derived via GCD. As expected the highest errors (ave. of 3–4mm) are observed at young (3–4mo.) mandibles. The

Subject (Age*)	1(34)		2(60)			3(36)			4(144)			5(72)			6(84)	
Age (mo.)	16	23	7	23	56	5	17	32	25	62	131	3	4	21	9	21
Ave. (mm)	2.1	2.3	2.1	1.8	1.7	2.1	2.2	1.4	2.5	2.8	2.7	4.0	3.2	2.0	2.7	3.0
Std. (mm)	1.2	1.2	1.4	1.5	1.1	1.0	1.6	1.5	1.5	1.4	1.5	2.7	1.6	1.3	1.7	2.0

Table 1. The average and standard deviations of the errors for each scanning of subject 1–6. Age* is the age in months at which the barycentric coordinates are derived. The errors measure the agreement between the biological landmarks and the correspondence derived via GCD.

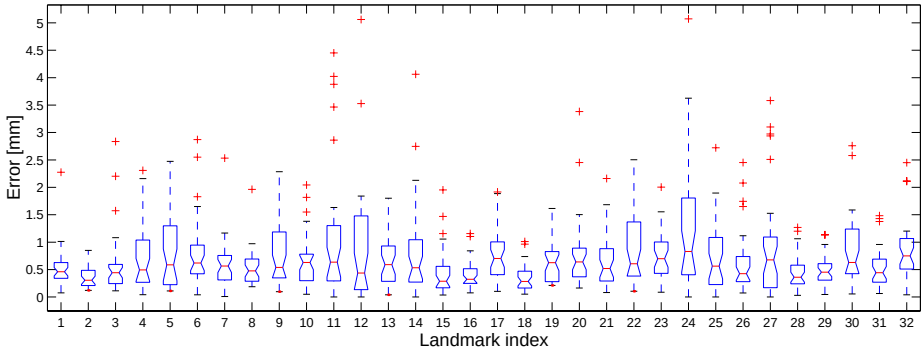

Fig. 1. Intra-observer residual variance related to each biological landmark.

total average of the errors over all landmarks is 2.1mm, well within the prediction errors reported for growth modelling in [1]. To examine the reproducibility of the landmark annotation the intra-observer variance is evaluated, see results in Figure 1. The precision is very high, with an average of 0.6mm, but possible bias and consistent trends in the errors remains unaccounted for due to the lack of independent observer repetitions. The discrepancy in correspondence is within acceptable limits when taking into account the possible error sources; i) the biological landmarks are placed in CT scans of varying in-plane resolution down to 0.5mm, ii) the unaccounted inter-observer variability, iii) the bias of manual segmentation, smoothing and closing of holes in the surface representation of the mandibles, and iv) the error in the recovery of the rigid body and free deformation when mapping the landmarks from the CT scanning onto the skeletal surfaces. Figure 2 shows the barycentric landmarks for patient 1–6 on the reference mandible applied in the GCD registration in [1].

To examine the underlying distribution and the inter-correlations of the biological landmarks in a coordinate independent frame of reference we apply two-set Canonical Correlations Analysis (CCA). CCA maximizes the correlation between linear combinations of two multivariate groups of variables, see [5, 14, 16]. We jointly analyse pairs of landmark variables $(\boldsymbol{x}, \boldsymbol{y})$, with dispersions $\boldsymbol{\Sigma}_{11}$ and $\boldsymbol{\Sigma}_{22}$ and cross-covariance $\boldsymbol{\Sigma}_{12} = \boldsymbol{\Sigma}_{21}{}^T$, and find sets of linear combinations (called canonical variates, CVs) of the zero mean original variables that maximize correlation $\rho = \mathrm{Corr}\{\boldsymbol{a}^T\boldsymbol{x}, \boldsymbol{b}^T\boldsymbol{y}\}$, under $\boldsymbol{a}^T\boldsymbol{\Sigma}_{11}\boldsymbol{a} = \boldsymbol{b}^T\boldsymbol{\Sigma}_{22}\boldsymbol{b} = 1$. Solving the generalized eigenvalue problems

$$\rho^2 = \frac{\boldsymbol{a}^T\boldsymbol{\Sigma}_{12}\boldsymbol{\Sigma}_{22}^{-1}\boldsymbol{\Sigma}_{21}\boldsymbol{a}}{\boldsymbol{a}^T\boldsymbol{\Sigma}_{11}\boldsymbol{a}} = \frac{\boldsymbol{b}^T\boldsymbol{\Sigma}_{21}\boldsymbol{\Sigma}_{11}^{-1}\boldsymbol{\Sigma}_{12}\boldsymbol{b}}{\boldsymbol{b}^T\boldsymbol{\Sigma}_{22}\boldsymbol{b}} \tag{2}$$

provides the subspaces of maximum correlation. Determining the canonical variates is done by projecting $\boldsymbol{x}$ respectively $\boldsymbol{y}$ onto the subspaces spanned by the eigenvectors, ρ is the canonical correlations between the new variates. The CCA analysis indicates three primary clusters of the biological landmarks; 1–6 relate to the chin, 7–19 and 20–32 relate to structures connected to the ramus

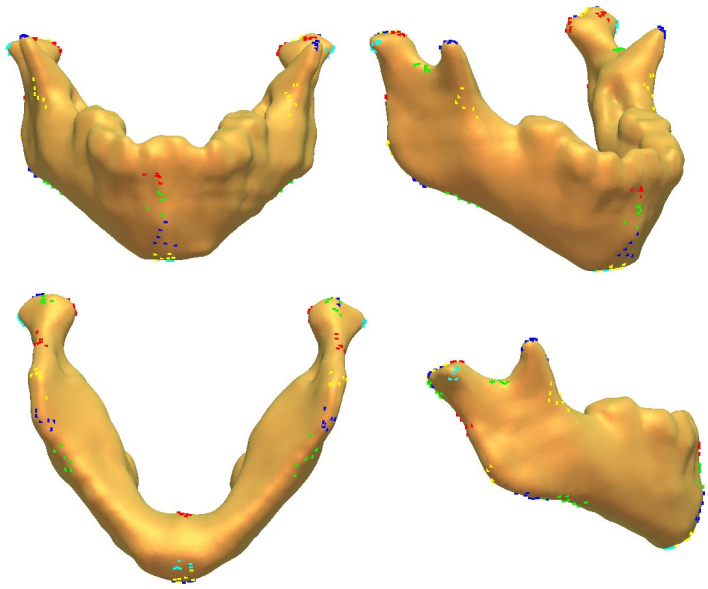

Fig. 2. Barycentric landmarks for patient 1–6 projected onto the reference mandible applied in the GCD registration. The colouring of the 32 landmarks is index dependent.

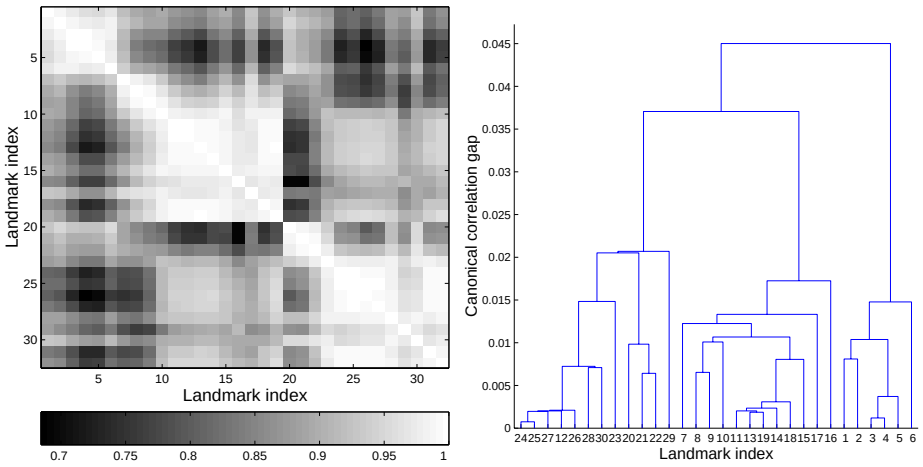

Fig. 3. Left: Canonical correlations of the 32 biological landmarks. Right: Hierarchical clustering using single linkage of the landmarks, the canonical correlations are applied as similarity measure.

of the mandible distributed on subclusters near the angle of the mandible, and the condylar and coronoid process, see Figure 3. The CCA based clustering of the landmarks is thus in agreement with the established biological atlas of the mandibular sections. The clustering of landmarks is also indicated in the error

distribution of the individual landmarks over all scans showing similar Jack-Saw patterns for the second and third primary group (results not shown).

3 Active Shape Growth Modelling

The set of biological landmarks is applied in a statistical shape analysis in pursuit of a growth model that correlates to centroid size of the shapes. The shapes are aligned by a generalized Procrustes analysis. A pure shape model is built using a similarity transformation in the Procrustes alignment, alternatively a rigid-body transformation may be used to build a size-and-shape model, [8]. An ASM is typically constructed based on a PCA of the Procrustes aligned shapes. Let each aligned shape be represented as a vector of concatenated x, y and z coordinates $\mathbf{x}_i = [x_{i1}, y_{i1}, z_{i1}, \ldots, x_{in}, y_{in}, z_{in}]^T$, $i = 1, \ldots, s$, where n is the number of vertices and s is the number of shapes. The PCA is performed on the shape matrix $\boldsymbol{X} = [(\mathbf{x}_1 - \overline{\mathbf{x}})| \ldots |(\mathbf{x}_s - \overline{\mathbf{x}})]$, where $\overline{\mathbf{x}}$ is the average shape. A new shape exhibiting the variance observed in the training set is constructed by adding a linear combination of eigenvectors to the average shape $\mathbf{x}_{new} = \overline{\mathbf{x}} + \boldsymbol{\Phi}\mathbf{b}$, where $\mathbf{b}$ is a vector of weights controlling the modes of shape variation and $\boldsymbol{\Phi} = [\phi_1|\phi_2| \ldots |\phi_t]$ is the matrix of the first t eigenvectors of the dispersion of the tanget space coordinates. Notice, that by correcting the data for patient specific mean shapes we remove inter-patient variability before projecting into tangent space and thus focus the ASM on shape and form variation. This furthermore produces a more compact model in tangent space with the first three components explaining 60, 69, and 73% of the total accumulated variance over 49, 58, and 66% without patient specific mean correction. Figure 4 shows a pairs plot of the subject, centroid size, and PCA1–3 component scores. Only PCA1 correlates to centroid size with a coefficient of 76%. By PCA we solely focus on obtaining a basis that has the maximum likelihood of reconstructing the training data. In the present case, PCA correlates to growth. However, this may not be the case in other studies. Instead, we propose to decompose the dynamics in shape space by turning to regression based techniques. In particular, we wish to search for dominating shape variations that show high correlation to growth measured by centroid size. The method of partial least squares (PLS) thus becomes a natural choice for shape variation decomposition. PLS is closely related to CCA. In PLS $R = \mathrm{Cov}\{\boldsymbol{a}^T\boldsymbol{x}, \boldsymbol{b}^T\boldsymbol{y}\}$ (here $\boldsymbol{x}$ is an observation in the tangent space and $\boldsymbol{y}$ often a scalar response variable) is maximized with another choice of constraints, namely $\boldsymbol{a}^T\boldsymbol{a} = \boldsymbol{b}^T\boldsymbol{b} = 1$ leading to

$$R^2 = \frac{\boldsymbol{a}^T\boldsymbol{\Sigma}_{12}\boldsymbol{\Sigma}_{21}\boldsymbol{a}}{\boldsymbol{a}^T\boldsymbol{a}} = \frac{\boldsymbol{b}^T\boldsymbol{\Sigma}_{21}\boldsymbol{\Sigma}_{12}\boldsymbol{b}}{\boldsymbol{b}^T\boldsymbol{b}}, \tag{3}$$

[12]. In this case matrix inversion is not needed which is valuable if we have many variables and few observations. Only the first pair of canonical variates (or latent variables) are calculated and the response CV is regressed on the predictor CV.

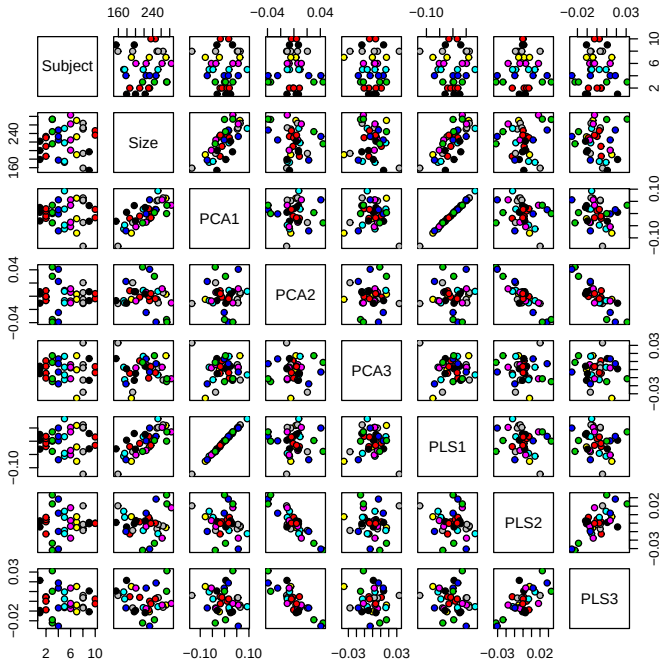

Fig. 4. Pairs plot of the patient index, the centroid size, the PCA1–3 and the PLS1–3 components.

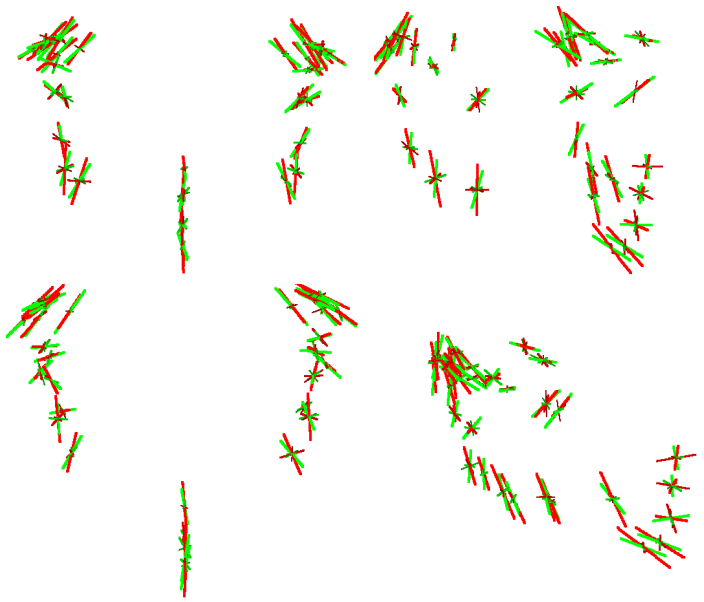

Fig. 5. The first three modes of variation using the PCA (red) and PLS (green) decomposition ranging from the mean shape ±3 std.

If more information is present in the residuals these are subtracted from the original response variables by means of multiple regression, and the predictor variables are projected into a subspace orthogonal to the solution found, and more iterations are performed, see also [9, 13]. In Figure 4 the scores for the PLS based decomposition is shown using centroid size as the dependent variable in the regression. Notice that PLS1 has almost a one-to-one correspondence to PCA1, but possesses slightly higher correlation to centroid size of 77%. The PLS study thus confirms that growth of the mandible is primarily contained in a one-dimensional linear component in Procrustes tangent space. This is in agreement with the findings in [1, 11] and does not conflict with the non-linear growth observed in biological coordinate references systems, [4]. In Figure 5 we show the first three modes of shape variation of the mean shape ± 3 standard deviations (std.) for both the PCA and the PLS components. The PCA and PLS components are shown in red and green respectively . The arrows decrease in width and brightness for increasing mode-index. Notice the overall agreement in the orientation of the primary modes.

4 Conclusion

A set of mandibular surfaces registered by approximately 15000 semi-landmarks using Geometry Constrained Diffusion is evaluated using 32 biological clinically identified landmarks based on distinct skeletal surface features. The robustness of the annotation is evaluated and compared to the correspondence derived using Geometry Constrained Diffusion. The registrations are found to be in good agreement under the expected degrees of uncertainty, and the study thus constitutes a clinical validation of the automated derived dense correspondence. A Canonical Correlation Analysis, extended to handle three dimensional landmarks and invariant under affine translations, detects that the biological landmarks naturally separate into different groups. A hierarchical clustering analysis shows the specific grouping of the individual landmarks in agreement with the established anatomical atlas of the mandible. The biological landmarks are applied in an Active Shape Model for which the principal mode of variation is highly correlated to growth measured by centroid size. This indicates that growth of the mandible is linear in Procrustes tangent space which confirms the finding in previous studies of the mandible surface represented by semi-landmarks. Finally, we extend the traditional Principal Components decomposition of the shape space by a novel approach targeting growth modelling directly. This is done by applying Partial Least Squares regression on the tangent space coordinates against the measured centroid size. The results are in good agreement with the previous findings of a single dominating one dimensional shape component correlatated to growth. However, the regression based decomposition is able to obtain a higher correlation since it directly searches for biological shape variation showing high covariation wrt. size and growth. The new approach generalizes to include multivariate dependent variables, and thus represents a generic framework for analyses and understanding of modes of variation in biological dynamical data.

Acknowledgments

The authors would like to thank Dr. Per R. Andresen (formerly IMM, DTU) for the initial segmentation and GCD registration of the data, and the Danish Technical Research Council for the supporting grant no. 26-01-0198.

References

1. P. R. Andresen, F. L. Bookstein, K. Conradsen, B. K. Ersbøll, J. Marsh, and S. Kreiborg. Surface-bounded growth modeling applied to human mandibles. *IEEE Transactions on Medical Imaging,*, 19(11):1053–1063, dec 2000.
2. P. R. Andresen and M. Nielsen. Non-rigid registration by geometry-constrained diffusion. In *Medical Image Computing and Computer-Assisted Intervention - MICCAI*, pages 533–543. Springer, 1999.
3. P. J. Besl and N. D. McKay. A method for registration of 3d shapes. *IEEE Transactions on Pattern Analysis and Machine Intelligence*, 14(2), 1992.
4. A Björk and V Skieller. Normal and abnormal growth of the mandible. A synthesis of longitudinal cephalometric implant studies over a period of 25 years. *Eur. J. Orthodontics*, 5:1–46, 1983.
5. W. W. Cooley and P. R. Lohnes. *Multivariate Data Analysis*. John Wiley and Sons, New York, 1971.
6. T. F. Cootes, G. J. Taylor, D. H. Cooper, and J. Graham. Training models of shape from sets of examples. In *British Machine Vision Conference: Selected Papers 1992*, Berlin, 1992. Springer-Verlag.
7. T.F. Cootes, D. Cooper, C.J. Taylor, and J. Graham. Active shape models - their training and application. *Comp. Vision and Image Understanding*, 61(1):38–59, 1995.
8. I.L. Dryden and K.V. Mardia. *Statistical Shape Analysis*. Wiley, Chichester, 1997.
9. I. E. Frank and J. H. Friedman. A statistical view of some chemometrics regression tools. *Technometrics*, 35(2):109–135, 1993.
10. J.C. Gower. Generalized Procrustes analysis. *Psychometrika*, 40:33–51, 1975.
11. K. B. Hilger, R. Larsen, and M. Wrobel. Growth modeling of human mandibles using non-euclidean metrics (to appear). *Medical Image Analysis*, 2003.
12. Klaus Baggesen Hilger. *Exploratory Analysis of Multivariate Data*. PhD thesis, Department of Informatics and Mathematical Modelling, Technical University of Denmark, 2001.
13. A. Höskuldsson. PLS regression methods. *Jour. of Chemometrics*, 2:211–228, 1986.
14. Harold Hotelling. Relations between two sets of variates. *Biometrika*, XXVIII:321–377, 1936.
15. S Kreiborg, H Aduss, and M M Cohen Jr. Cephalometric study of the Apert syndrome in adolescence and adulthood. *J. Craniofacial Genetics Develop. Biol.*, 19:1–11, 1999.
16. R. Larsen and K. B. Hilger. Statistical shape analysis using non-euclidean metrics (to appear). *Medical Image Analysis*, 2003.
17. M. Nielsen, P. Johansen, A.D. Jackson, and B. Lautrup. Brownian warps: A least committed prior for non-rigid registration. In *Medical Image Computing and Computer-Assisted Intervention - MICCAI*, pages 557–564. Springer, 2002.